



Performance of bremsstrahlung refits for converted photons

Summer Student Programme 2011

July 19th - September 08th

Summer Student:

LUIGI LONGO

Supervisors:

KERSTIN TACKMANN

MARCOS JIMENEZ BELENGUER

Abstract

In the ATLAS experiment, the results of three different track fitters are available for converted photons: the default algorithm (or *Global χ^2 track fitter*), the *Gaussian Sum Filter* and the *Dynamic Noise Adjustment*. Each of these uses a different method to take into account the bremsstrahlung effects. However, while the default χ^2 fitter treats every track as pion and hence underestimates bremsstrahlung effects for electrons, the other two algorithms implement dedicated strategies for taking into account bremsstrahlung losses for electrons. The aim of this topic will be to study and to compare the performance of these fitters for converted photons.

Contents

1	Introduction	3
2	Photon conversions	3
2.1	Bremsstrahlung	4
3	Track fitters	5
3.1	The Global χ^2 track fitter	5
3.2	Kalman Filtering	6
3.2.1	Gaussian Sum Filter	6
3.2.2	Dynamic Noise Adjustment	7
4	Samples and cuts	8
4.1	Weights	11
5	Analysis	12
5.1	Fraction of the conversion candidates in the tail VS p_t regions	16
5.2	Fraction of the conversion candidates in the tail VS eta regions	19
5.3	Crystal Ball peak and sigma for different p_t regions	20
6	Conclusion	21

1 Introduction

The photon conversion reconstruction in the ATLAS detector is an important tool for different physics measurements involving electromagnetic decay products: having an efficient reconstruction of converted photons, in fact, enhances the efficiency of detection of particles with di-photon final states, such as the Higgs boson.

Because of the fact that the interaction of the photons with the tracker is completely dominated by e^+ and e^- pair production¹, for the reconstruction it is necessary to consider, together with the electron scattering in the material, the effect due to bremsstrahlung. The *Global χ^2 track fitter*, the *Gaussian Sum Filter* (GSF) and the *Dynamic Noise Adjustment* (DNA) are three different fitters developed to solve this problem and performed now as part of the standard reconstruction software in the ATLAS experiment: however, while the χ^2 fitter is used as the default algorithm, the others are provided in addition and should yield improved results.

In this topic, after a brief introduction about the physics behind the photon conversion, the aim of the work will be to study and to compare the three fitters focusing the attention on double-track conversions.

2 Photon conversions

For photons with energy above 1 GeV the cross section for the conversion process is almost completely independent of the photon energy [1]. It may be written in the following way

$$\sigma = \frac{7A}{9X_0N_A} \quad (1)$$

where A is the atomic mass of the target given in g/mol, $N_A = 6.022 \times 10^{23}$ is the Avogadro's number and X_0 is the radiation length².

On the other hand, the differential cross section for photon conversions, in terms of the quantity $x = \frac{E_e}{E_\gamma}$ (electron energy over photon energy), is given by

$$\frac{d\sigma}{dx} = \frac{A}{X_0N_A} \left(1 - \frac{4}{3}x(1-x)\right). \quad (2)$$

¹Since the photons which are relevant to physical measurements have energies above 1 GeV, all the other interaction between the photons and the tracker material, such as Compton and Rayleigh scattering, can be ignored: at this energy, in fact, they have a cross section several orders lower than the photon conversion [1].

²For elements heavier than helium the radiation length may be approximated from the atomic mass A and the atomic number Z by the following relation

$$X_0 = \frac{716.4 \text{ g cm}^{-2} A}{Z(Z+1) \ln(287\sqrt{Z})}.$$

Since the cross section is symmetric in x and $1 - x$, you have that the photon momentum is not shared equally between the electron and the positron. It is therefore possible that a fraction of the photon conversions is highly asymmetric and one, either the electron or the positron, is produced with a very low energy: in particular, if this energy falls below the threshold required to produce a reconstructable track in the ATLAS tracker, the converted photon will have only one track reconstructed and it will be difficult to distinguish a γ from a single electron or positron.

2.1 Bremsstrahlung

In the reconstruction algorithm it is important to remember that, like heavy particles, electrons and positrons also suffer a collisional energy loss when they go through matter. However, because of their small mass³, an additional energy loss mechanism comes into play [2]: the emission of electromagnetic radiation arising from scattering in the electric field of a nucleus or, better said, *bremsstrahlung*.

While at energies of a few MeV or less this process is still a relatively small factor, as the energy is increased, the probability of bremsstrahlung quickly shoots up. Loss of energy by radiation, at few 10's of MeV, is comparable to or greater than the collision-ionization loss and then, at energy above the *critical energy*⁴, the bremsstrahlung dominates completely: at this point you will observe, as consequence, the reduction of the electron curvature radius as shown in Fig. 1.

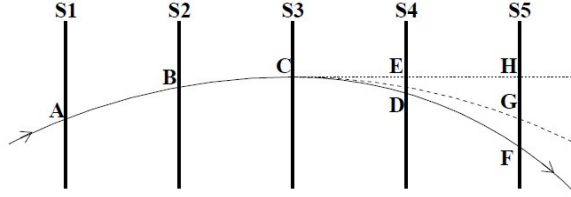


Figure 1: If an electron emits a photon at point C, its track will have a smaller curvature radius after that point and it will hit layer S5 at point F instead of point G, while the photon follows the tangent C-E-H [3].

The probability density that the electrons keep their direction and a fraction z of their energy is given by the Bethe-Heitler distribution $f(z)$ (Fig. 2): it depends on the amount of traversed material and is highly asymmetric, with a singularity at $z \rightarrow 1$ and a long tail extending to very small z [3].

³The emission probability varies as the inverse square of the particle mass.

⁴For each material it is possible to define a critical energy, E_c , through the following expression

$$\left(\frac{dE}{dx} \right)_{rad} \Big|_{E=E_c} = \left(\frac{dE}{dx} \right)_{coll} \Big|_{E=E_c}.$$

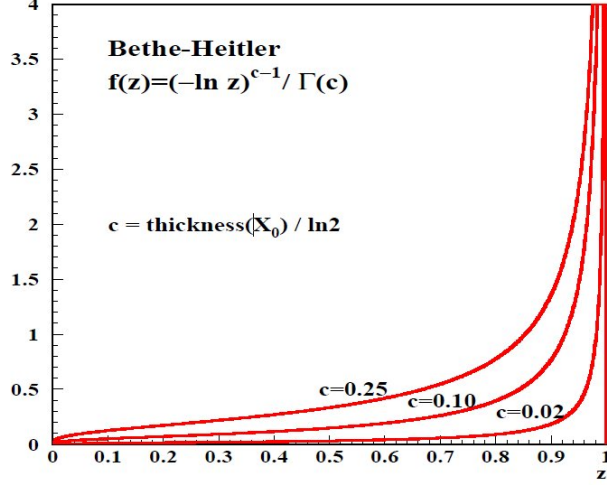


Figure 2: Bethe-Heitler distribution of the fraction z of energy retained by the radiating electron[3].

3 Track fitters

In the ATLAS experiment three different algorithms are performed for the track reconstruction: the *Global χ^2 track fitter*, the *Gaussian Sum Filter* (GSF) and the *Dynamic Noise Adjustment* (DNA). Each of these takes into account the bremsstrahlung effect in a different way. In particular, whereas the default algorithm can only estimate the energy losses, the other algorithms try to take into account the variation in the curvature radius during the reconstruction: it is for this reason that they are called *brem fitter*. However, before discussing these bremsstrahlung fitters, it is useful to show, after the Global χ^2 track fitter, how the Kalman Filter (KF) works: both GSF and DNA are, in fact, based on the latter.

3.1 The Global χ^2 track fitter

The Global χ^2 track fitter is the default algorithm used by the ATLAS experiment [4]. It only needs an initial estimate of the track parameter and, to consider the energy loss⁵ together with the scattering, it uses this particular χ^2 form

$$\chi^2 = \sum_{meas} \frac{r_{meas}^2}{\sigma_{meas}^2} + \sum_{scat} \left(\frac{\theta_{scat}^2}{\sigma_{scat}^2} + \frac{(\sin \theta_{loc})^2 \varphi_{scat}^2}{\sigma_{scat}^2} \right) + \sum_{Eloss} \frac{(\Delta E - \overline{\Delta E})^2}{\sigma_{Eloss}^2} \quad (3)$$

where r_{meas} is a residual (the difference between a measurement and the track prediction obtained by propagating the track through the magnetic field to a measurement), θ_{scat} and φ_{scat} are the scattering angles at scattering layer (the difference in angle between

⁵Considering the energy losses is a way to take into account the bremsstrahlung effects.

the incoming and outgoing track), ΔE is the fitted energy loss at a material layer and $\overline{\Delta E}$ is the expected energy loss obtained from the material description.

In this algorithm, after the residuals and their derivatives have been calculated, the track parameters are updated using the update formula: this process continues until there is no appreciable difference between the new and the old χ^2 .

3.2 Kalman Filtering

The Kalman Filter [3] is an iterative procedure used to determine the vector of track parameter, y , and its covariance matrix, C , considering the measurement m and its covariance matrix V at each detector layer k . The procedure includes three steps:

1. extrapolate y and C from layer $k - 1$ to layer k

$$y_{k-1} \rightarrow y_k^-, \quad C_{k-1} + Q_{k-1} \rightarrow C_k^- \quad (4)$$

where Q_k is the covariance matrix of the system noise at layer k , which takes into account things like multiple scattering and bremsstrahlung;

2. calculate Kalman gain K at layer k

$$K_k = \frac{C_k^-}{C_k^- + V_k}; \quad (5)$$

3. do measurement update

$$y_k = y_k^- + K_k(m_k - y_k^-), \quad C_k = (1 - K_k)C_k^-. \quad (6)$$

It can be demonstrated that this procedure only works properly if both measurement uncertainty V and the process noise Q are well described by Gaussian distribution: for this reason, while it is useful in the case of measurement errors and multiple scattering, it's certainly not for bremsstrahlung.

3.2.1 Gaussian Sum Filter

The Gaussian Sum Filter [3] is a non-linear generalization of the KF. It approximates the Bethe-Heitler distribution by a weighted mixture of several Gaussians in order to take into account the asymmetry and the low-energy tail of the distribution (Fig. 3).

For every component a different KF is executed and the results are merged together, using the new weights calculated during the process, to obtain the track parameter vector and its covariance matrix. In addition, since the number of the components grows at every hit added, a reduction of components is performed at each step.

However, due to the less precise hit measurement in the TRT, the GSF fit is only performed for tracks with silicon hits.

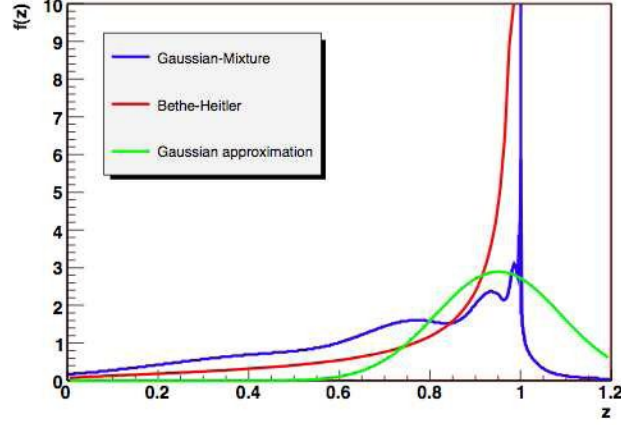


Figure 3: Comparison between the Bethe-Heitler distribution, a single Gaussian distribution of equivalent mean and r.m.s., a sum of several Gaussian used by the GSF[3].

3.2.2 Dynamic Noise Adjustment

For the DNA [3], a fit is performed to flag hits which may be associated with bremsstrahlung. This fit tries to estimate the increase in curvature due to possible bremsstrahlung at the current detector layer. If no bremsstrahlung was flagged, the track fitter reverts to the default Kalman filtering procedure. Otherwise, the results of single parameter fit -the estimated fraction of energy retained by the electron, z - is used to calculate the additional effective "system noise" term, which is then fed to the Kalman filter.

The effective "system noise" variance calculation is illustrated by Fig. 4, which shows how the Bethe-Heitler distribution is mapped onto the Gaussian distribution of unit width. The deviation Δz of estimated z from the medium z_0 is mapped onto a Gaussian to find the corresponding deviation Δx . The effective noise σ is then calculated as $\sigma_{DNA}(z) = \Delta z / \Delta x$.

This procedure is equivalent to representing the random variable z , distributed according to the Bethe-Heitler probability density, in the form

$$z = z_0 + x\sigma_{DNA}(z) \quad (7)$$

where x is a random variable with Gaussian probability distribution.

At the end the variance σ_{DNA}^2 is added to the appropriate term of the Kalman covariance matrix used during the fit, similarly to the treatment of any other source of system noise. Also in this case, as in GSF algorithm, the fit is only performed for tracks with silicon hits.

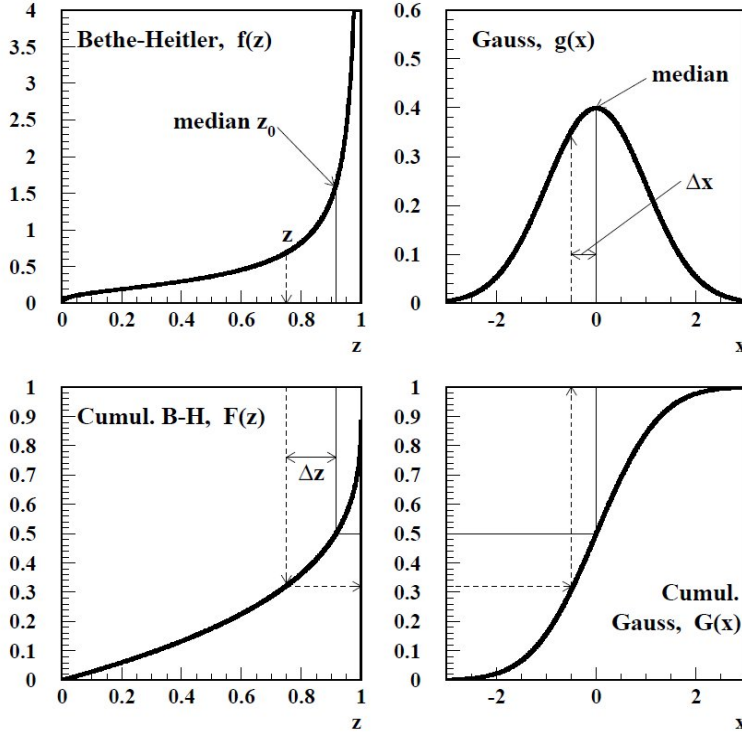


Figure 4: Mapping of the probability distributions used to calculate the variance of the effective noise term [3].

4 Samples and cuts

To study the different fitters, three different samples have been used: two MC samples and a data sample. For the MC samples we have considered the DP and JF samples. In both samples background has been simulated but while for the first one the fraction of real photons is increased by a generator level filter, in order to have a large statistics for real signal, the second one does not use it: JF contains a similar background to that of data (Fig. 4) and, in particular, it has been possible to find that its background is overestimated.

However, in order to have enough statistic for the analysis, we have considered different kind of DP and JF, as shown in the table 4, for different p_t range.

Then the following selection has been applied to obtain the sample of photon conversions used in this study

Double-track conversions : since the photon momentum estimation becomes worse when you lose an electron or positron track during the photon reconstruction (see sec. 2), the idea is to consider only those photons with 2 reconstructed tracks after the conversion.

Good eta range : photon candidates in the following ranges $0 < |\eta| < 1.37$ and $1.52 <$

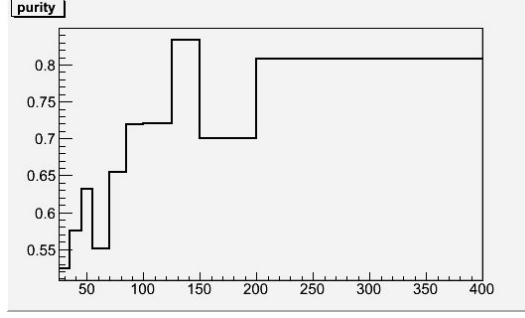


Figure 5: *Purity* (number of real reconstructed photons over all reconstructed photons) of JF sample is shown for different p_t regions (see sec. 3): because of background overestimation, it is worse in JF than in data.

DP	JF	p_t range used (GeV)
mc10b_7TeV_DP17	mc10b_7TeV_JF17	[20,45]
mc10b_7TeV_DP35	mc10b_7TeV_JF35	[45,85]
mc10b_7TeV_DP70	mc10b_7TeV_JF70	[85,200]
mc10b_7TeV_DP140	mc10b_7TeV_JF140	[200,400]
mc10b_7TeV_DP280	mc10b_7TeV_JF240	[400,1000]

Table 1: Different samples used in the analysis for the different p_t range.

$|\eta| < 2.37$ have been considered in order to skip the crack region where you have a degraded resolution because of the calorimetry geometry⁶.

Author : this variable is defined during the reconstruction step and gives information about the algorithm used: those photons, reconstructed by the standard photon reconstruction (author==4) or also as electrons (author==16), have been analyzed [5].

Photon and OQ cleaning : photons, that have been reconstructed using bad quality clusters or fake clusters originating from calorimeter problems, have been rejected [5].

Tight selection : the tight photon requirement are optimized to provide good rejection of the π_0 background (see Tab 2): in particular the cut thresholds are chosen in order to provide an identification efficiency around 85% and to minimize the corresponding fake rate [6].

Isolation cut : in the ATLAS experiment the calorimeter variables $EtConeXX$ are calculated by taking a simple sum of the calorimeter cell energies inside of a cone of

⁶Photons candidates are required to lie in the pseudorapidity region covered by the finely segmented part of the first layer of the electromagnetic calorimeter [6].

a certain radius around the cluster barycenter, excluding a 5×7 grid of cells in the center of the cone. There are (at least) two effects that modify this value in unwanted ways that are important to take into account [5]:

- a photon or electron will leak some of its energy outside of this central core and will cause the isolation energy to grow as a function of E_t ;
- soft energy deposits from pile-up interactions will change the isolation energy depending on the amount of activity in the current event (*in-time pileup*) as well as previous events (*out-of-time pileup*).

On the base of different corrections used, different variables can be defined from EtConeXX: however for the purpose of this analysis, according to the reference [7], only the following cut has been used $\text{EtCone40} < 5 \text{ GeV}$.

Successful refit : a successful fit is required with the GSF and DNA to have a consistent sample of conversions for all three track fitters.

At this point, while the data sample is ready for the analysis, for the MC other cuts have been considered. However, whereas for the DP sample there has been only the request of having photons from hard process (*truthmatch cut*), for the JF, using again this kind of cut, different selections have been performed to obtain the following samples

- JF: it is the sample with the first cuts but without the truthmatch cut;
- JFwith: it is the JF sample with the truthmatch cut;
- background: it is the sample made of photon candidates not truth matched to real photons.

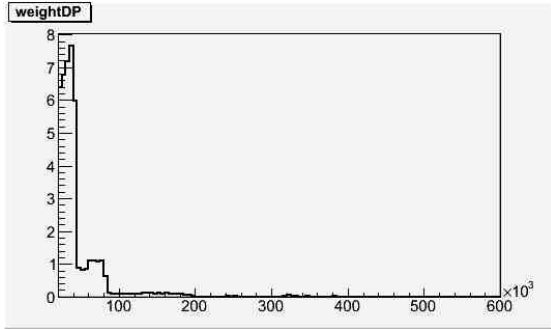
Category	Description	Name
Acceptance	$ \eta < 2.37, 1.37 < \eta < 1.52$ excluded	—
Hadronic leakage	· Ratio of E_t in the first sampling of the hadronic calorimeter to E_t of the EM cluster(used over the range $ \eta < 0.8$ and $ \eta > 1.37$)	R_{had_1}
	· Ratio of E_t in all the hadronic calorimeter to E_t of the EM cluster $0.8 < \eta < 1.37$)	R_{had}
EM Middle layer	· Ratio in η of cell energies in 3×7 versus 7×7 cells	R_η
	· Lateral width of the shower	ω_2
	· Ratio in φ of cell energies in 3×3 and 3×7 cells	R_φ

Category	Description	Name
EM Strip layer	· Shower width for three strips around maximum strip	ω_{s3}
	· Total lateral shower width	ω_{stot}
	· Fraction of energy outside core of three central strips but within seven strips	F_{side}
	· Difference between the energy associated with the second maximum in the strip layer and the energy reconstructed in the strip with the minimal value found between the first and second maxima	ΔE
	· Ratio of the energy difference associated with the largest and second largest energy deposits over the sum of these energies	E_{ratio}

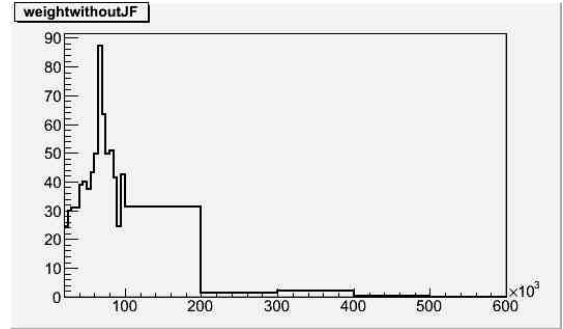
Table 2: Variables used for tight photon identification cuts [6].

4.1 Weights

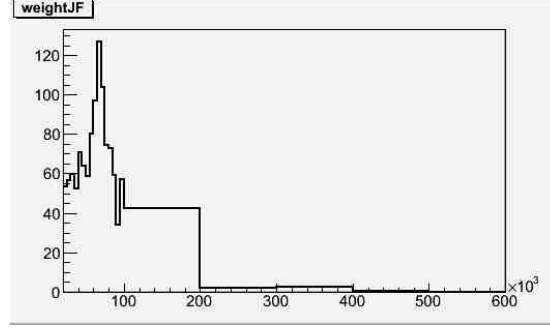
In order to reproduce the same p_t shape as in data, each event in the different samples has been weighted: in particular the weights have been estimated as the ratio of the data over MC events for every bin. However, because of the smaller statistics in the JF samples, a different binning has been used for the JF and DP samples, as you can see in Fig. 6.



(a) DP weights



(b) JF weights



(c) JFwith weights

Figure 6: Weights of the different samples used.

However, since the fig. 6(b) and 6(c) reach big values in the first bins, both the plot have been scaled by the quantity

$$\frac{\text{MaxXvalue} - \text{MinXvalue}}{\sum_{\text{bin}} \text{BinContent} \times \text{BinLength}}$$

before being used in the analysis.

5 Analysis

During the analysis, using the variables

ph_cl_E : energy reconstructed by the calorimeter, that can be use as reference since in data you obviously do not know the true momentum,

ph_conv_p : momentum reconstructed by the ID using the default fitter,

ph_conv_GSF_p : momentum reconstructed by the ID using the GSF fitter,

ph_conv_DNA_p : momentum reconstructed by the ID using the DNA fitter,

the quantities $\frac{\text{ph_cl_E}}{\text{ph_conv_p}}$, $\frac{\text{ph_cl_E}}{\text{ph_conv_GSF_p}}$ and $\frac{\text{ph_cl_E}}{\text{ph_conv_DNA_p}}$ have been defined for different η and p_t regions (see Tab. 3).

They play an important role to understand how the bremsstrahlung fitters work. The distributions show a Gaussian core, due to the momentum resolution, and a long tail, due to the bremsstrahlung: as the bremsstrahlung effect grows, in fact, there is a momentum underestimation and, as consequence, an overestimation of the previous quantities.

At this point, once you have these distributions, it is possible to perform a fit (see Fig. 7)

η region		p_t region	
DP/data	JF/JFwith	DP/data	JF/JFwith
0-0.6	0-0.6	25-35 GeV	25-35 GeV
0.6-1.37	0.6-1.37	35-45 GeV	35-45 GeV
1.52-1.81	1.52-1.81	45-55 GeV	45-55 GeV
1.81-2.37	1.81-2.37	55-70 GeV	55-400 GeV
		70-85 GeV	
		85-100 GeV	
		100-125 GeV	
		125-150 GeV	
		150-400 GeV	

Table 3: η and p_t regions: while for eta the same regions have been selected for all the samples, four p_t ranges have been chosen for JF and JFwith because of the smaller statistics.

using the *Crystal Ball function*⁷ to measure the number of conversion candidates in the tail⁸ over all the conversion candidates for every p_t and eta region : it is, in fact, one of the parametrization which gives good enough results to compare different samples and algorithms when the bremsstrahlung effect is present⁹.

⁷The Crystal Ball function is made of a Gaussian core and a power-law low-end tail, after a threshold, and, together with its derivative, it is continuous. It is given by

$$f(x; \alpha_{CB}, n_{CB}, \bar{x}_{CB}, \sigma_{CB}) = \text{NBC} \cdot \begin{cases} e^{-\frac{(x-\bar{x}_{CB})^2}{2\sigma_{CB}^2}} & \text{for } \frac{x-\bar{x}_{CB}}{\sigma} > -\alpha_{CB} \\ \left(\frac{n_{CB}}{|\alpha_{CB}|}\right)^{n_{CB}} e^{-\frac{|\alpha_{CB}|^2}{2}} \left(\frac{n_{CB}}{|\alpha_{CB}|} - |\alpha_{CB}| - \frac{x-\bar{x}_{CB}}{\sigma_{CB}}\right)^{-n_{CB}} & \text{for } \frac{x-\bar{x}_{CB}}{\sigma} < -\alpha_{CB} \end{cases}$$

where NBC is a normalization factor, \bar{x}_{CB} is the peak of the Gaussian, σ_{CB}^2 is the variance of the Gaussian, α_{CB} is the distance between the peak of the Gaussian and the starting point of the tail in σ_{CB} unit and n_{CB} is the parameter that describes the power-law of the tail [8].

⁸Starting point of the tail is given by $\bar{x}_{CB} - \alpha_{CB} \cdot \sigma_{CB}$.

⁹It is possible also to consider the number of conversion candidates in the core of the Gaussian over all the conversion candidates with the core defined as the region between $\bar{x}_{CB} - 2\sigma_{CB}$ and $\bar{x}_{CB} + 2\sigma_{CB}$: in the analysis this method has been used to check the results and, as expected, no difference has been found.

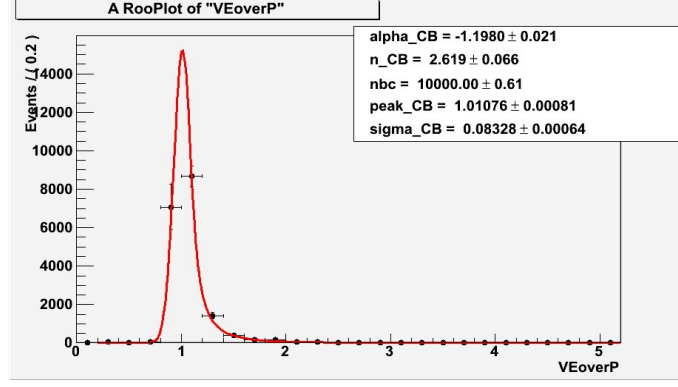
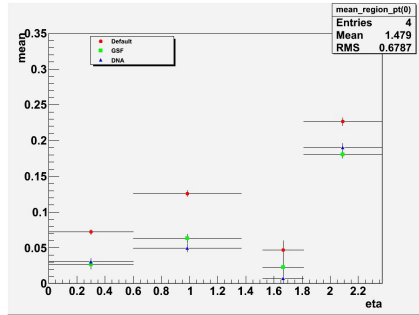


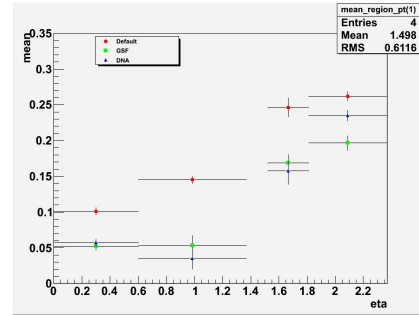
Figure 7: Fit performed for the DP sample in the p_t range $[25,35]$ GeV and η range $[0,0.6]$.

Resolution

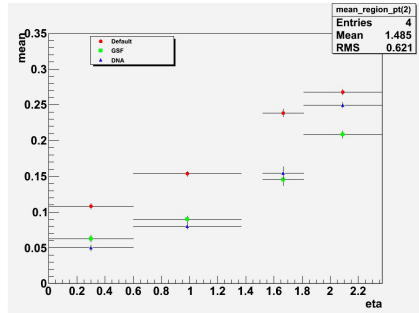
Before studying the behaviour of the E/p distribution, it is informative to look at the resolution, defined as $\Delta p = \frac{E_{tr}-p}{E_{tr}}$, in a MC sample in order to have a general idea about how the different algorithms work, for every p_t and eta bin: in particular the mean of the distribution of Δp and its error have been estimated for real photons using the DP sample (Fig. 8).



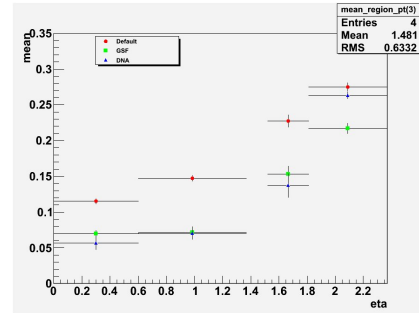
(a) $p_t \in [25, 35]$ GeV



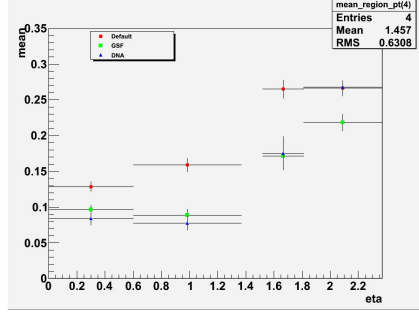
(b) $p_t \in [35, 45]$ GeV



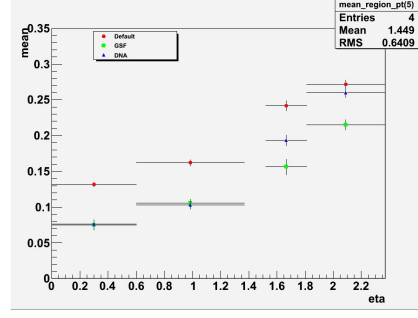
(c) $p_t \in [45, 55]$ GeV



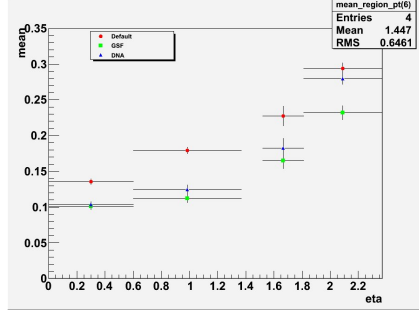
(d) $p_t \in [55, 70]$ GeV



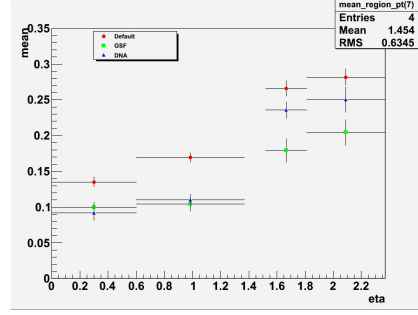
(e) $p_t \in [70, 85]$ GeV



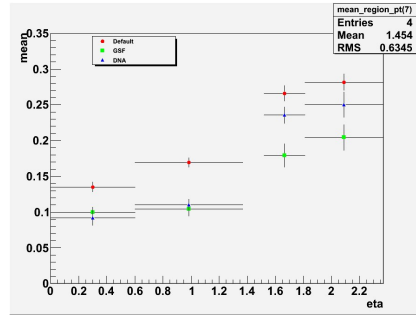
(f) $p_t \in [85, 100]$ GeV



(g) $p_t \in [100, 125]$ GeV



(h) $p_t \in [125, 150]$ GeV



(i) $p_t \in [150, 400]$ GeV

Figure 8: Resolution versus $|\eta|$ for different p_t regions (DP sample).

Both the GSF and the DNA show better behaviour, that is a mean closer to zero, than the default track fit: however, while the GSF is performing better at high η and p_t , the DNA is performing better at low values.

In addition to evaluating the behaviour of the track fitters on the MC, studying E/p will allow for a comparison of the track fitters using data.

Background

Using JF, JFwith and background, it is possible to get an idea of the effect of background on the E/p distribution. In particular if you look at Fig. 9 you observe the shift of the peak, the increase of the sigma and, also, of the conversion candidates in the tail.

The same thing happens if you consider other p_t and eta regions.

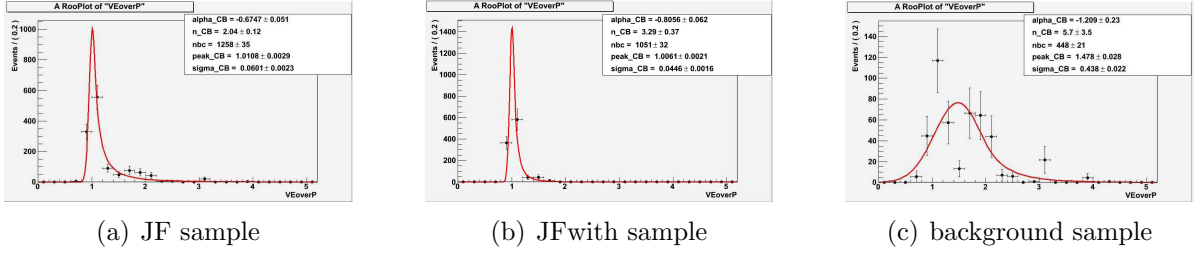
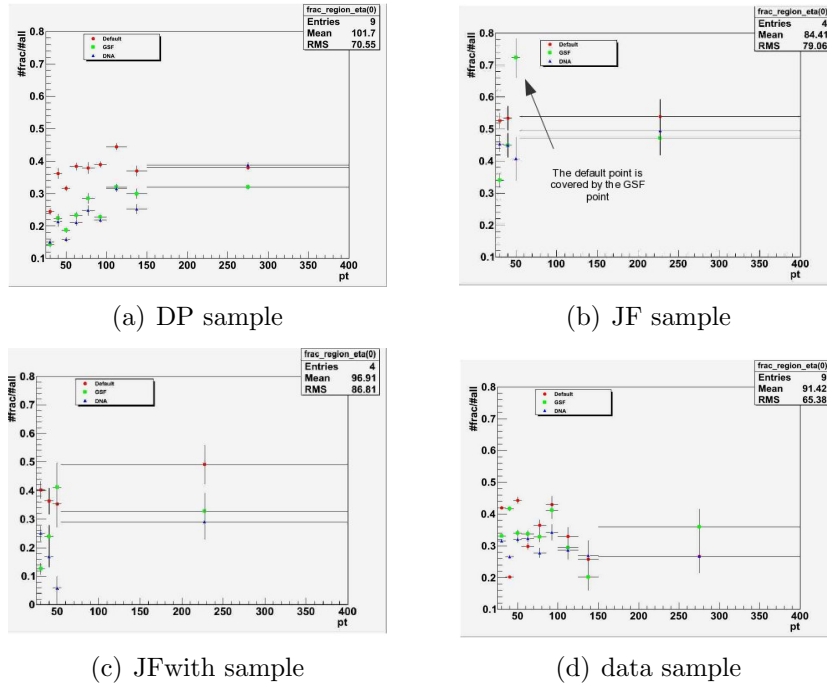


Figure 9: JF, JFwith and background for $p_t \in [25, 35]$ GeV and for $|\eta| \in [0, 0.6]$.

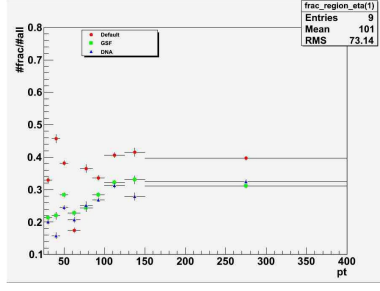
5.1 Fraction of the conversion candidates in the tail VS p_t regions

For each sample the fraction of the conversion candidates in the tail has been determined in bins of η and p_t and is shown in Fig. 5.1

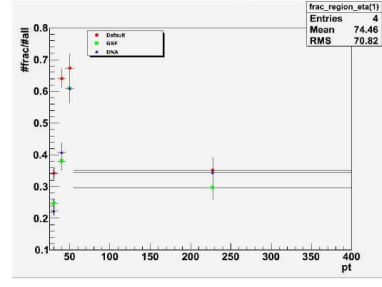
$|\eta| \in [0, 0.6]$



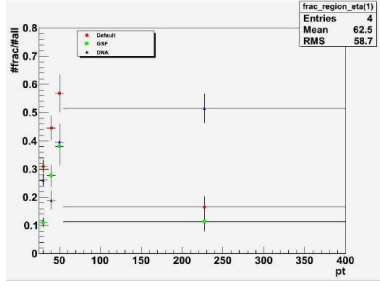
$$\cdot|\eta| \in [0.6, 1.37]$$



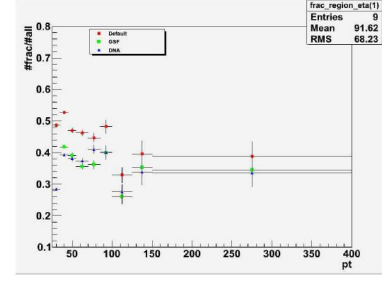
(e) DP sample



(f) JF sample

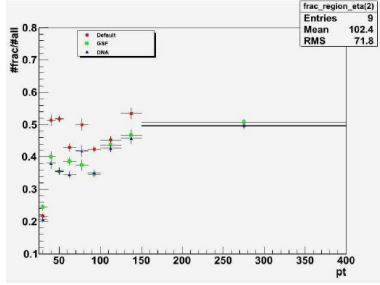


(g) JFwith sample

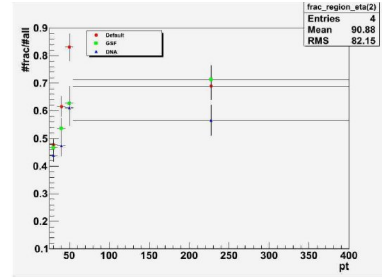


(h) data sample

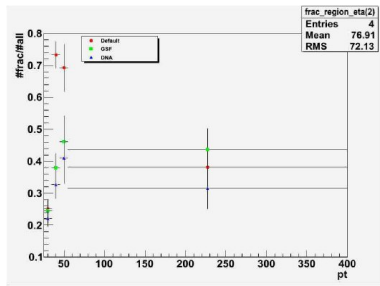
$$\cdot|\eta| \in [1.52, 1.81]$$



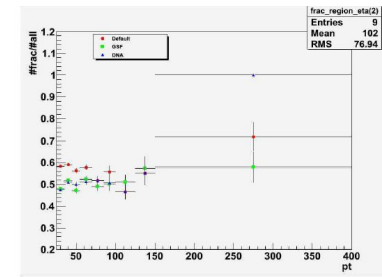
(i) DP sample



(j) JF sample



(k) JFwith sample



(l) data sample

$$\cdot|\eta| \in [1.81, 2.37]$$

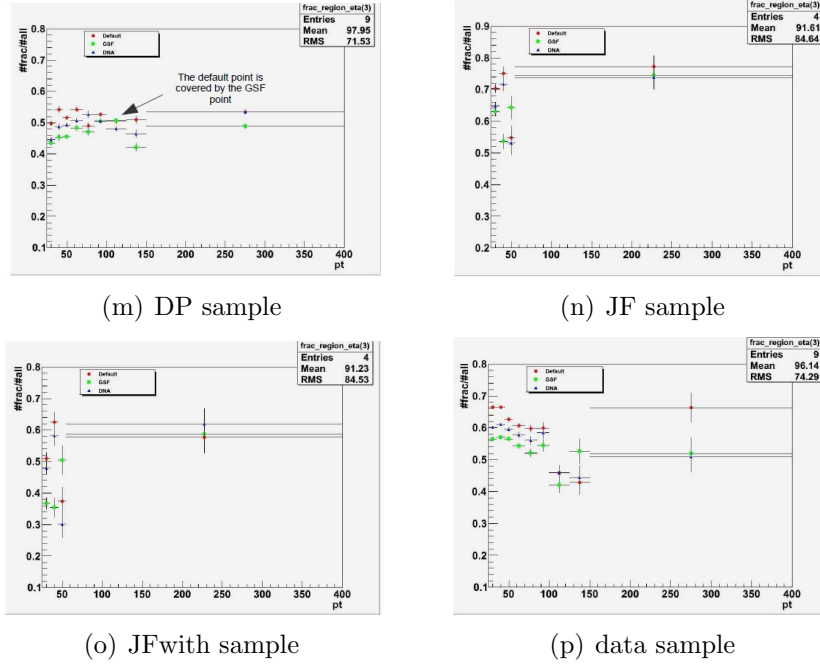


Figure 10: Fraction of the conversion candidates in the tail VS p_t for the different samples studied and for the different η region.

In agreement with what has been observed for the resolution using the DP sample, the GSF and DNA provide a better estimate of the momentum of the conversion than the default fit: in fact, after refitting the tracks with the GSF and the DNA, the fraction of conversions in the tail of E/p distribution is significantly reduced in all η and p_t regions. In a few instances, the default fit seems to display a smaller fraction of conversions in the tail. These cases can be traced back to badly fitted E/p distributions, as demonstrated in Fig. 10(d).

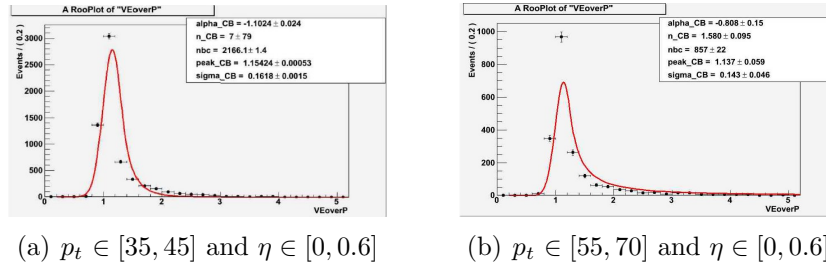


Figure 11: Examples of bad fit: because of the bad fit performance less conversion candidates in the tail are measured and, as consequence, the χ^2 algorithm seems better than the others.

Also for the DNA algorithm you can see the same fit problem in Fig. 10(1) (data sample): in this case the fit is so bad that only the tail is performed and, as result, you can see the fraction of the tail near 100% (Fig. 12).

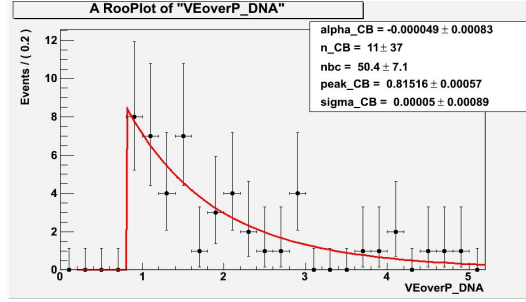


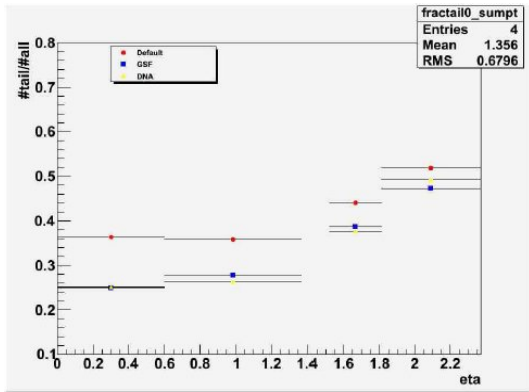
Figure 12: Example of bad fit for DNA algorithm.

Anyway, as observed in the study of the resolution, it is possible to observe again how the GSF seems work better than DNA for high η and p_t regions and the contrary for the low values.

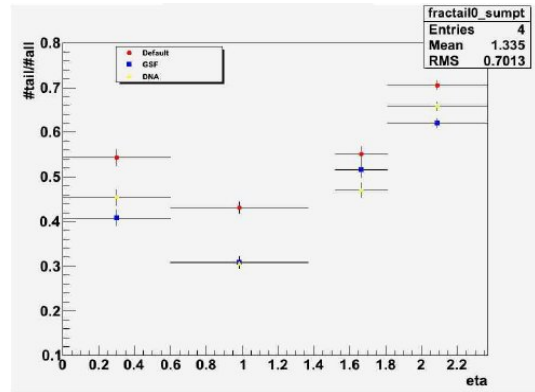
In addition, studying the behaviour of E/p on JF samples, the following effect is observed when comparing samples with and without background: the fraction of the conversion candidates in the tail is bigger in the sample with background than the other (Fig. 10(b)-Fig 10(c), Fig. 10(f)-Fig 10(g), Fig. 10(j)-Fig 10(k), Fig. 10(n)-Fig 10(o)).

5.2 Fraction of the conversion candidates in the tail VS eta regions

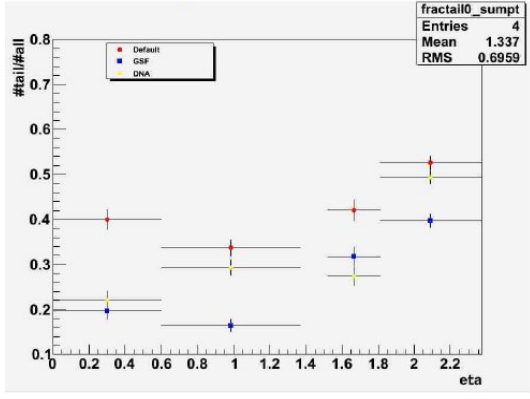
As additional cross check, another kind of analysis has been used: integrating over p_t , the fraction of the conversions in the tail has been measured as function of η as shown in Fig. 13



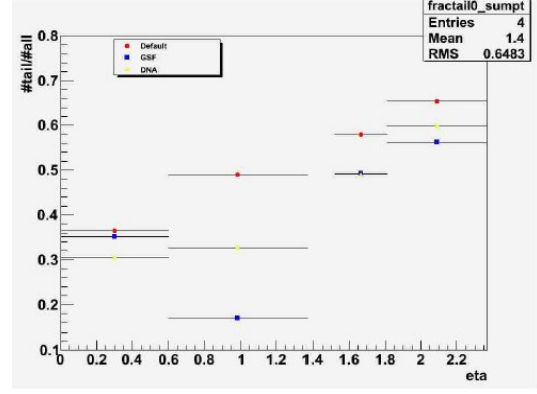
(a) DP sample



(b) JF sample



(c) JFwith sample



(d) data sample

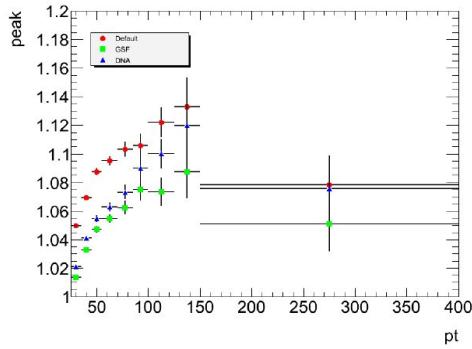
Figure 13: Fraction of the conversion candidates in the tail vs η for the different samples.

The same results of the previous section can be observed: the DNA and GSF are better than the default algorithm, but it is hard to demonstrate that one of them is better than the other, and the JF sample is shifted because of the presence of background.

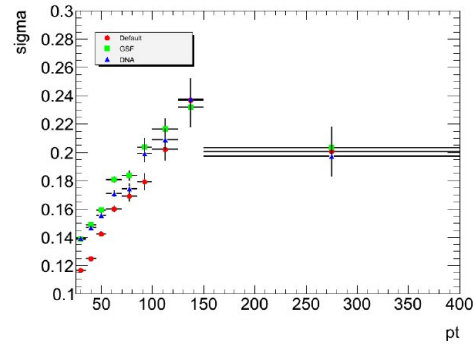
5.3 Crystal Ball peak and sigma for different p_t regions

Two other quantities are of interest:

- Crystal ball peak vs p_t (Fig. 14(a));
- Crystal ball sigma vs p_t (Fig. 14(b)).



(a) peak vs p_t



(b) sigma vs p_t

Figure 14: Peak position and Gaussian sigma of the Crystal Ball fits to the different E/p distributions observed on data. The same trend as shown here is also visible for the simulation samples.

Since the distribution peak should be near 1, it is possible to use consistency with 1 as measure of fit performance for the different p_t region; the sigma VS p_t plot, instead, can be used to have an idea about the resolution.

While the previous results showed a better performance of the bremsstrahlung fitters compared to the default fit, without allowing to favour one of the bremsstrahlung fitters, the GSF shows a better performance with respect to the peak position.

The sigma plot, instead, shows that the resolution gets worse with increasing p_t for all fitters: while the GSF Gaussian core is the widest, the default algorithm core is the narrowest.

6 Conclusion

During this analysis the performance of the bremsstrahlung refits for converted photons was studied using the quantities 'energy measured by the calorimeter over momentum estimated by the ID using the different bremsstrahlung fitters'.

A better performance has been found for the GSF and DNA compared to the default ATLAS algorithm. In particular it has also been found that the GSF fitter is better than DNA for high p_t and high η and the contrary for low p_t and η but, looking only at the peak of the fit for different p_t regions, it seems that GSF is the best bremsstrahlung fitter.

The bremsstrahlung refits could find application in the following areas:

- improvement of the $H \rightarrow \gamma\gamma$ mass resolution combining calorimeter and tracker measurement of the energy and using the bremsstrahlung refitted conversion for the mass reconstruction;
- the bremsstrahlung fitter could improve the mass resolution through the pointing;
- use improved E/p distribution in the purity estimation for converted photons.

References

- [1] ATLAS collaboration; Expected Performance of ATLAS Experiment, Detector, Trigger and Physics, Electrons and Photons; Dec. 2008.
- [2] William R. Leo; Techniques for nuclear and particle physics experiments: a how-to approach; Springer 1994.
- [3] Evelina Bouhova-Thacker, Vakhtang Kartvelishvili; Electron bremsstrahlung recovery in ATLAS tracking using Dynamic Noise Adjustament; PoS (ACAT) 046.
- [4] T G Cornelissen, M Elsing, I Gavrilenko, J-F Laporte, W Liebig, M Limper, K Nikolopoulos, A Poppleton, A Salzburger The Global χ^2 track fitter in ATLAS; 2008 J. Phys.: Conf. Ser. 119 032013.
- [5] ATLAS collaboration; <https://twiki.cern.ch>.
- [6] ATLAS collaboration; Expected photon performance in the ATLAS experiment; Apr. 2011.
- [7] Mike Hance, Jamie Saxon, Brig Williams (University of Pennsylvania); $H \rightarrow \gamma\gamma$; Apr. 2011.
- [8] John Erthal Gaiser; Charmonium Spectroscopy from radiative decays of the J/ψ and ψ' , appendix-F; Aug. 1982.